After cultivation with bacteria, the specimen was rinsed with PBS(–) and immersed into a 2.5% glutaraldehyde solution for 2 hr for fixation. The specimens were rinsed with PBS(–) again and immersed into an ethidium bromide solution (2 μg/ml; Molecular Probes, Carlsbad, CA, U.S.A.) for 5 min for the staining of bacterial nucleic acid in biofilms [26]; they were then immersed into a fluorescein isothiocyanate (FITC)-conjugated concanavalin A solution (50 μg/ml; Sigma-Aldrich, St. Louis, MO, U.S.A.) for 3 min for the staining of polysaccharides in biofilms [1, 30]. A CLSM (LSM 5 PASCAL; Carl Zeiss MicroImaging GmbH, Jena, Germany) was used for fluorescent observation. The observation was carried out for 10 specimens.

Measurement of the number of bacteria by ATP assay: An ATP-dependent luminescence reaction between luciferin and luciferase was utilized to count the number of bacteria [20, 21]. After incubation, the specimen was rinsed with PBS(–). Subsequently, ATP in the bacterial cytoplasm was extracted by sonication for 10 min from the specimen immersed in 0.5 ml of 0.5% trichloroacetic acid solution. The amount of ATP was measured using an ATP assay kit (ENLITEN ATP Assay System Bioluminescence Detection Kit; Promega, Madison, WI, U.S.A.) and a luminometer (Auto Lumat; EG&G Berthold, Bad Wildbad, Germany). The relations between the number of bacteria measured by a hemocytometer for bacterial counting (A161; SLGC, Tokyo, Japan) and the relative light unit (RLU) measured by the ATP assay system were established for the respective bacteria. Utilizing these standard relations, the RLU values measured in the experiments were converted to the numbers of bacteria. The measurements were carried out for 10 specimens.

Statistical analysis: The obtained data were analyzed by two-way ANOVA to determine the effectiveness of PMB coating and antibiotics in decreasing the number of bacteria. Subsequently, statistical differences among cases in the noncoated and PMB-coated surfaces were examined by Scheffe's multiple comparison test.

RESULTS

CLSM observation: Figure 2 shows the example of a typical observation by CLSM. In every case of exposure to *S. aureus*, *S. epidermidis*, and *P. aeruginosa*, many bacteria and polysaccharides were revealed to exist on the noncoated surfaces of the specimens, as shown in Figs. 2(a), 2(c), and 2(e). On the other hand, there was little or no trace of bacteria or polysaccharides on MPC-coated surfaces, as shown in Figs. 2(b), 2(d), and 2(f). Accordingly, we concluded that biofilm was formed on the noncoated surfaces whereas no biofilm was formed on MPC-coated surfaces.

Number of bacteria measured by ATP assay: The ATP assay was performed to measure the number of bacteria and the data are presented in Table 1. Furthermore, statistical analysis was carried out and significant differences between the experimental groups were examined. The analyzed results are illustrated in Fig. 3. In the cases of *S. aureus* and *S. epidermidis*, application of either kind of antibiotics decreased the number of bacteria on the noncoated surfaces ($p<0.01$). On the PMB-coated surfaces, their numbers were smaller than those on the noncoated surfaces ($p<0.01$). The application of antibiotics further decreased the number ($p<0.01$). In the cases of *P. aeruginosa*, application of gentamicin decreased the number ($p<0.01$) whereas cefazolin increased the number of bacteria ($p<0.01$) on the noncoated surfaces. On the PMB-coated surfaces, their numbers were smaller than those on the noncoated surfaces ($p<0.01$). The application of gentamicin decreased the number ($p<0.01$) whereas cefazolin increased the number ($p<0.01$).

DISCUSSION

Device-associated infections are caused by the bacteria adhered to internal prosthetic devices and are thought to occur through many critical steps [3, 7, 10, 18, 22]. These steps are as follows: adsorbance of various molecules, including peptides and proteins, onto the surfaces of the devices; the mediation of bacterial attachment via these molecules; and the formation of biofilms. If biofilm formation is completed, the bacteria in the biofilm are protected from the biological defense mechanism, and furthermore, from the administered antibacterial agents. Hence, the formation of biofilms on the surface of devices establishes a refractory infection, i.e., device-associated infections [6, 8, 19, 24, 27, 28].

The MPC polymer has the phospholipid polar group and the methacryloyl group in its molecular structure. This confers MPC excellent polymerization ability. The MPC polymers have desirable properties for the inhibition of protein adsorption and cell adhesion. Recently, the MPC polymer was utilized for the coating of medical devices such as artificial blood vessels, implantable artificial hearts, and artificial lungs and successful preventions of thrombus formation were reported [13–17, 25]. Since the attachment of bacteria to the material's surface is also mediated by adsorbed proteins, MPC might be most favorably utilized to inhibit the formation of biofilms. In this investigation, we utilized the PMB as an MPC polymer for the coating materials of metallic specimens to explore the possible uses for the prevention of device-associated infections.

S. aureus, *S. epidermidis*, and *P. aeruginosa* were chosen for this experiment since these bacteria are the most common species causing device-associated infections in the field of orthopedics, and they are also implicated in the pathogenesis of osteomyelitis [10]. Their cultivation was performed following the biofilm formation assay established in previous reports [1, 9, 27, 30]. Then the specimens were stained with ethidium bromide for bacterial nucleic acid and (FITC)-conjugated concanavalin A for polysaccharides and examined by a CLSM, which was also adopted in the biofilm formation assay [1, 26, 30].

In the experiments, the observations by a CLSM clearly demonstrated the presence of bacteria and the existence of polysaccharides on the noncoated surfaces of specimens, as

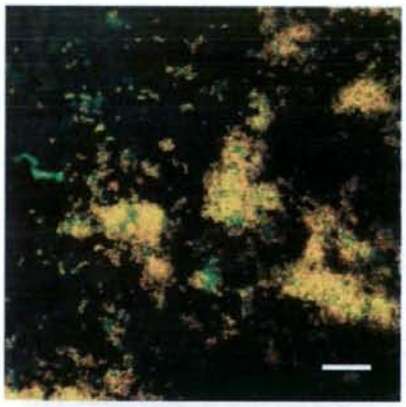

(a) *S. aureus* on noncoated surface

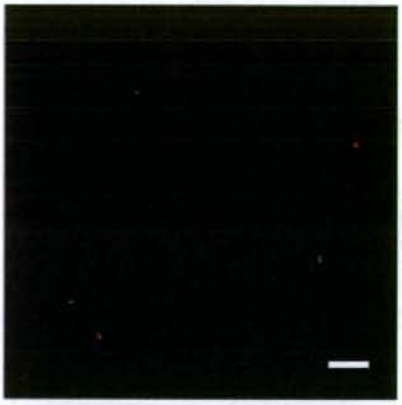

(b) *S. aureus* on PBM-coated surface

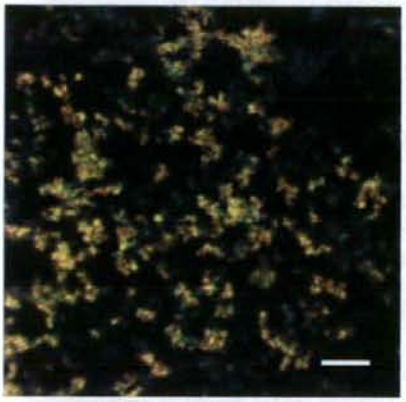

(c) *S. epidermidis* on noncoated surface

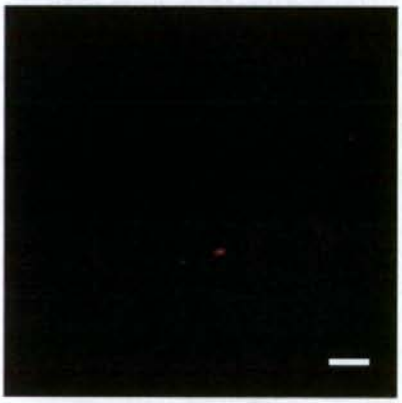

(d) *S. epidermidis* on PMB-coated surface

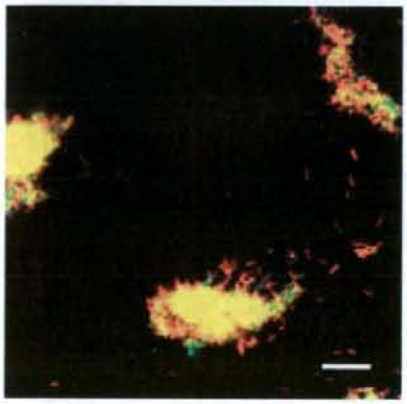

(e) *P. aeruginosa* on noncoated surface

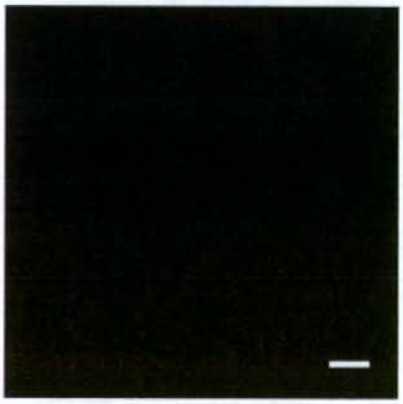

(f) *P. aeruginosa* on PMB-coated surface

Table 1. Number of bacteria (10^5 cells/specimen) on noncoated and PMB-coated surfaces on specimens after 24 hr incubation in which antibiotics were absent or either cefazolin or gentamicin were added, following 24 hr incubation without antibiotics. The values are represented as mean ± SD

coating antibiotics	none	none cefazolin	gentamicin	none	PMB coating cefazolin	gentamicin
S. aureus	2702 ± 303	1722 ± 200	1621 ± 91	163.3 ± 9.6	1.469 ± 0.305	1.263 ± 0.134
S. epidermidis	41.99 ± 6.27	1.677 ± 0.186	1.789 ± 0.249	0.8291 ± 0.1099	0.4283 ± 0.0486	0.3172 ± 0.0357
P. aeruginoza	2008 ± 263	6080 ± 385	1278 ± 295	29.74 ± 2.12	48.92 ± 2.37	9.209 ± 0.345

shown in Figs. 2(a), 2(c), and 2(e), which provided a morphological evidence of the formation of biofilms.

The number of bacteria was measured by the ATP assay, and it was demonstrated that the number of bacteria on the noncoated surface of the specimens decreased with statistical significance following the application of cefazolin or gentamicin in the cases of *S. aureus*, as shown in Fig. 3(a). However, the application of antibiotics did not even halve the number of bacteria. The number of *P. aeruginosa* was not halved by the antibiotics in a similar manner as shown in Fig. 3(c). Contrastively, the number of bacterial was increased when they were cultivated in the cefazolin added medium. This might be attributed to that the specimens were incubated for 24 hr in medium without antibiotics and then they were incubated for another 24 hr in new medium containing cefazolin, to which *P. aeruginosa* was not susceptible. In either case of bacteria, anyhow, the fact that antibiotics could not halve the bacteria provided a functional evidence of the formation of biofilms, in which the bacteria were enveloped and protected from the antibiotics. On the other hand, the number of *S. epidermidis* bacteria on the noncoated surface was decreased to less than 1/10 times of the original number by the application of the antibiotics, as shown in Fig. 3(b). The biofilms formed by *S. epidermidis* were seemingly less effective in protecting the bacteria.

In contrast, on the PMB-coated surfaces, the bacteria and polysaccharides were not detected by confocal laser microscopy, as shown in Figs. 2(b), 2(d), and 2(f); this provided a morphological evidence of the absence of biofilms.

The ATP assay demonstrated that the number of bacteria on the PMB-coated surfaces of the specimens decreased with statistical significance compared to those on noncoated surfaces. Although the number of bacteria decreased approximately only 1/20 times the original number in the cases of *S. aureus*, the application of antibiotics further decreased the number of bacteria to approximately 1/2000 times, as shown in Fig. 3(a). This phenomenon proved that the bacteria are not protected from antibiotics and implies that *S. aureus* on the PMB-coated surface, which could not be removed by rinsing, did not form a biofilm. Similarly, the number of *S. epidermidis* was decreased to approximately 1/50 times the original number on the PMB-coated surface, and the application of antibiotics further decreased the number to approximately 1/1200 times, as shown in Fig. 3(b). The number of *P. aeruginosa* was decreased to approximately 1/70 times on a PMB-coated surface, and the application of gentamicin further decreased the number to approximately 1/220 times, but cefazolin was not effective in reducing the number of bacteria, as shown in Fig. 3(c). The difference in the response toward cefazolin and gentamicin is explained by the fact that cefazolin is a beta-lactam antibiotic, which is active against gram-positive bacteria such as *Staphylococcus* sp. but not against *P. aeruginosa*, and gentamicin is an amino-glycoside antibiotic that is active against gram-negative bacteria, including *P. aeruginosa* as well as gram-negative bacteria.

Hence, the observed decreases in the number of bacteria by the application of antibiotics provided a functional evidence that PMB coating prevented the formation of biofilms.

Thus, we concluded that the PMB coating effectively prevented the formation of bacterial biofilms on the surface of metallic specimens. Although our results were limited to *in vitro* experiments and further investigations are necessary, the decrease in the number of bacteria in the order of 1/100 to 1/1,000 is encouraging. We expect that the PMB coating combined with validated uses of antibiotics might provide an effective approach to the simultaneous achievement of a biocompatible surface of devices and the prevention of the device-associated infections.

Further investigations are necessary to achieve successful clinical applications. One of the issues to be examined is, durability of the coating. Yoneyama [32] implanted the MPC polymer coated artificial vessels made of polyester fibers to carotid arteries of rabbit, and observed the antithrombogenicity as long as 4 weeks after implantation. We confirmed the prevention of biofilm forming with the use of PMB coating in 48 hr experiments; however, verification of the durability should be performed. Furthermore, the toxicity of the polymer eluted from the coating layer should be examined.

Fig. 2. CLSM observations of the specimens with noncoated and PMB-coated surfaces after 48 hr incubation. (a) *S. aureus* on noncoated surface, (b) *S. aureus* on PMB-coated surface, (c) *S. epidermidis* on noncoated surface, (d) *S. epidermidis* on PMB-coated surface, (e) *P. aeruginosa* on noncoated surface, (f) *P. aeruginosa* on PMB-coated surface. The nucleic acid in bacteria was stained with ethidium bromide (red) and polysaccharide by FITC conjugated concanavalin A (green). Bar is 10 μm. Many bacteria and polysaccharides were detected on the noncoated surfaces, whereas they were very few on PMB-coated surfaces.

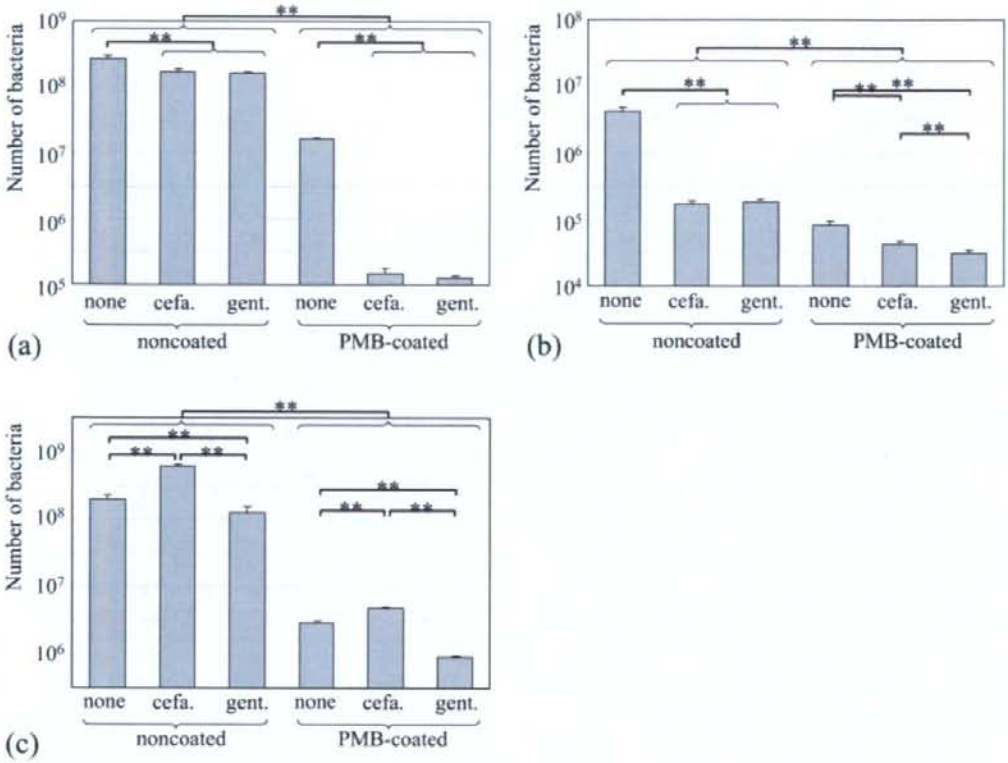

Fig. 3. Number of bacteria on noncoated and PMB-coated surfaces of specimens after 24 hr incubation in which antibiotics were absent or either cefazolin or gentamicin were added, following 24 hr incubation without antibiotics. (a) *S. aureus*, (b) *S. epidermidis*, (c) *P. aeruginosa*.

(a) Number of *S. aureus* on the surfaces on specimens. ** Significant difference ($p<0.01$) was observed; between noncoated and PMB-coated surfaces; between cases in which antibiotics were either absent or present on the noncoated and PMB-coated surfaces.

(b) Number of *S. epidermidis* on the surfaces on specimens. ** Significant difference ($p<0.01$) was observed; between noncoated and PMB-coated surfaces; between cases in which antibiotics were absent and cefazolin and gentamicin were added on the PMB-coated surfaces.

(c) Number of *P. aeruginosa* on the surfaces on specimens. ** Significant difference ($p<0.01$) was observed; between noncoated and PMB-coated surfaces; between cases in which antibiotics were absent, cefazolin and gentamicin were added on the noncoated and PMB-coated surfaces.

ACKNOWLEDGEMENT. This study was partially supported by Grants-in-Aid for Scientific Research on Priority Area (No.15086206) from the Ministry of Education, Culture, Sports, Science and Technology of Japan.

REFERENCES

1. Akiyama, H., Huh, W. K. and Fujii, K. 2002. Confocal laser microscopic observation of glycocalyx production by *Staphylococcus* aureus *in vitro*. *J. Dermatol. Sci.* **29**: 54–61.
2. Caldwell, D. E., Korber, D. R. and Lawrence, J. R. 1992. Confocal laser microscopy and digital image analysis. *Adv. Microb. Ecol.* **12**: 1–67.
3. Chang, C. C. and Merritt, K. 1994. Infection at the site of implanted materials with and without preadhered bacteria. *J. Orthop. Res.* **12**: 526–531.
4. Costerton, J. W., Lewandowski, Z., Caldwell, D. E., Korber, D. R. and Lappin-Scott, H. M. 1995. Microbial biofilms. *Annu. Rev. Microbiol.* **49**: 711–745.
5. Felten, A., Grandry, B., Lagrange, P. H. and Casin, I. 2002. Evaluation of three techniques for detection of low-level methicillin-resistant *Staphylococcus aureus* (MRSA): a disk diffusion method with cefoxitin and moxalactam, the Vitek 2 System, and the MRSA-Screen Latex Agglutination Test. *J. Clin. Micorbiol.* **40**: 2766–2771.
6. Gristina, A. G. 1987. Biomaterial centered infection. Microbial adhesion versus tissue integration. *Science* **27**: 1588–1595.
7. Harris, L. G., Foster, S. J. and Richards, R. G. 2002. An introduction to *Staphylococcus aureus*, and techniques for identify-

ing and quantifying *S. aureus* adhesions in relation to adhesion to biomaterials: review. *Eur. Cell Mater.* **4**: 39–60.
8. Harris, L. G., Tosatti, S. and Wieland, M. 2004. *Staphylococcus aureus* adhesion to titanium oxide surfaces coated with non-functionized poly(L-lysine)-grafted- poly(ethylene glycol) copolymers. *Biomaterials* **25**: 4135–4148.
9. Hirota, K., Murakami, K. and Nemoto, K. 2005. Coating of a surface with 2-methacryloyloxyethyl phosphorylcholine (MPC) co-polymer significantly reduces retention of human pathogenic microorganisms. *FEMS Microbiol. Lett.* **248**: 37–45.
10. Hudson, M. C., Ramp, W. K. and Frankenburg, K. P. 1999. *Staphylococcus aureus* adhesion to bone matrix and bone-associated biomaterials. *FEMS Microbiol. Lett.* **173**: 279–284.
11. Hussain, M., Hasting, J. G. and White, P. J. 1991. Isolation and composition of the extracellular slime made by coagulase-negative staphylococci in a chemically defined medium. *J. Infect. Dis.* **163**: 534–541.
12. Ishihara, K., Fukumoto, K., Iwasaki, Y. and Nakabayashi, N. 1999. Modification of polysulfone with phospholipid polymer for improvement of the blood compatibility. Part 1. Surface characterization. *Biomaterials* **20**: 1545–1551.
13. Ishihara, K., Oshida, H. and Endo, Y. 1992. Hemocompatibility of human whole blood on polymers with a phospholipid polar group and its mechanism. *J. Biomed. Mater. Res.* **26**: 1543–1552.
14. Ishihara, K., Ueda, T. and Nakabayashi, N. 1990. Preparation of phospholipid polymers and their properties as polymer hydrogel membranes. *Polym. J.* **22**: 355–360.
15. Ishihara, K., Ziats, N. P. and Tierney, B. P. 1991. Protein adsorption from human plasma is reduced on phospholipid polymers. *J. Biomed. Mater. Res.* **25**: 1397–1407.
16. Iwasaki, Y. and Ishihara, K. 2005. Phosphorylcholine-containing polymers for biomedical applications. *Anal. Bioanal. Chem.* **381**: 534–546.
17. Iwasaki, Y., Nakabayashi, N. and Ishihara, K. 2003. *In vitro* and *ex vivo* blood compatibility study of 2-methacryloyloxyethyl phosphorylcholine (MPC) copolymer-coated hemodialysis hollow fibers. *J. Artif. Organs* **6**: 260–266.
18. Jeanine, A., Jaques, O. G. and Anne, M. 1999. Tracking adhesion factors in *Staphylococcus caprae* strains responsible for human bone infections following implantation of orthopaedic material. *Microbiology* **145**: 2033–2042.
19. Jennings, D. A., Morykwas, M. J., Burns, W. W., Crook M. E., Hudson, W. P. and Argenta, L. C. 1991. *In vitro* adhesion of endogenous skin microorganism to breast prostheses. *Ann. Plast. Surg.* **27**: 216–220.
20. Lundin, A. and Thore, A. 1975. Analytical information obtainable by evaluation of the time course of firefly bioluminescence in the assay of ATP. *Anal. Biochem.* **66**: 47–63.
21. McElroy, W. D. and DeLuca, M. A. 1983. Firefly and bacterial luminescence. Basic science and applications. *J. Appl. Biochem.* **5**: 197–209.
22. Merritt, K. and Chang, C. C. 1991. Factors influencing bacterial adherence to biomaterials. *J. Biomater. Appl.* **5**: 185–203.
23. Merritt, K. and Dowd, J. D. 1987. Role of internal fixation in infection of open fracture: Studies with *Staphylococcus aureus* and *Proteus mirabilis*. *J. Orthop. Res.* **5**: 23–28.
24. Montanaro, L., Arciola, C. R. and Baldassarri, L. 1999. Presence and expression of collagen adhesion gene (can) and slime production in *Staphylpcoccus aureus* strains from orthopaedic prosthesis infection. *Biomaterials* **20**: 1945–1949.
25. Ogawa, R., Watanabe, J. and Ishihara, K. 2003. Domain-controlled polymer alloy composed of segmented polyurethane and phospholipid polymer for biomedical applications. *Sci. Technol. Adv. Mater.* **4**: 523–530.
26. Qian, Z., Stoodley, P. and Pitt, W. G. 1996. Effect of low-intensity ultrasound upon biofilm structure from confocal scanning laser microscopy observation. *Biomaterials* **17**: 1975–1980.
27. Ramage, G., Tunney, M. M. and Patrick, S. 2003. Formation of propinibacterium acnes biofilms on orthopaedic biomaterials and their susceptibility to antimicrobials. *Biomaterials* **24**: 3221–3227.
28. Sheehan, E., McKenna, J. and Mulhall, K. J. 2004. Adhesion of *Staphylococcus* to orthopaedic materials, an *in vivo* study. *J. Orthop. Res.* **22**: 39–43.
29. Takahashi, H. 2001. Examination about the bio-film formation prevention effect of the antibacterial new coating catheter material which blended citrate silver and lecithin. *Kansenshoushi* **75**: 678–685 (in Japanese).
30. Takenaka, S., Iwaku, M. and Hoshino, E. 2001. Artificial *Pseudomonas aeruginosa* biofilm and confocal laser scanning microscopic analysis. *J. Infect. Chemother.* **7**: 87–93.
31. Wassall, M. A., Santin, M. and Isalberti, C. 1997. Adhesion of bacterial to stainless steel and silver-coated orthopedic external fixation pins. *J. Biomed. Mater. Res.* **36**: 325–330.
32. Yoneyama, T., Ito, M., Sugihara, K., Ishihara, K. and Nakabayashi, N. 2000. Small diameter vascular prosthesis with a non-thrombogenic phospholipid polymer surface: preliminary study of a new concept for functioning in the absence of pseudo- or neointima formation. *Artif. Organs* **24**: 23–28.

ARTHRITIS & RHEUMATISM
Vol. 60, No. 1, January 2009, pp 166–178
DOI 10.1002/art.24243

Identification of the Core Element Responsive to Runt-Related Transcription Factor 2 in the Promoter of Human Type X Collagen Gene

Akiro Higashikawa, Taku Saito, Toshiyuki Ikeda, Satoru Kamekura, Naohiro Kawamura, Akinori Kan, Yasushi Oshima, Shinsuke Ohba, Naoshi Ogata, Katsushi Takeshita, Kozo Nakamura, Ung-il Chung, and Hiroshi Kawaguchi

Objective. **Type X collagen and runt-related transcription factor 2 (RUNX-2) are known to be important for chondrocyte hypertrophy during skeletal growth and repair and development of osteoarthritis (OA) in mice. Aiming at clinical application, this study was undertaken to investigate transcriptional regulation of human type X collagen by RUNX-2 in human cells.**

Methods. **Localization of type X collagen and RUNX-2 was determined by immunohistochemistry, and their functional interaction was examined in cultured mouse chondrogenic ATDC-5 cells. Promoter activity of the human type X collagen gene (COL10A1) was examined in human HeLa, HuH7, and OUMS27 cells transfected with a luciferase gene containing a 4.5-kb promoter and fragments. Binding to RUNX-2 was examined by electrophoretic mobility shift assay and chromatin immunoprecipitation.**

Results. **RUNX-2 and type X collagen were colocalized in mouse limb cartilage and bone fracture callus. Gain and loss of function of RUNX-2 revealed that RUNX-2 is essential for type X collagen expression and terminal differentiation of chondrocytes. Human COL10A1 promoter activity was enhanced by RUNX-2 alone and more potently by RUNX-2 in combination with the coactivator core-binding factor β in all 3 human cell lines examined. Deletion, mutagenesis, and tandem repeat analyses identified the core responsive element as the region between −89 and −60 bp (termed the hypertrophy box [HY box]), which showed specific binding to RUNX-2. Other putative RUNX-2 binding motifs in the human COL10A1 promoter did not respond to RUNX-2 in human cells.**

Conclusion. **Our findings indicate that the HY box is the core element responsive to RUNX-2 in human COL10A1 promoter. Studies on molecular networks related to RUNX-2 and the HY box will lead to treatments of skeletal growth retardation, bone fracture, and OA.**

Hypertrophic differentiation of chondrocytes during endochondral ossification is an essential step in skeletal growth and repair (1,2). We and others have reported that chondrocyte hypertrophy also contributes to cartilage degradation during the development of osteoarthritis (OA) (3–5). Type X collagen is a short, network-forming collagen specifically expressed by hypertrophic chondrocytes (6). The physiologic importance of type X collagen has been shown by the impairment of endochondral ossification and skeletal growth that results from loss of function of the type X collagen gene in mice (7–9). Similarly, mutations in the carboxy-terminal domain of the human type X collagen gene (COL10A1) cause a severe skeletal disorder called Schmid-type metaphyseal chondrodysplasia, with growth retardation, waddling gait, and OA (10–12). Hence, elucidation of the mechanisms regulating the type X collagen gene will contribute to understanding the molecular backgrounds of skeletal growth and repair and OA not only in mice, but also in humans.

Supported by a Grant-in-Aid for Scientific Research from the Japanese Ministry of Education, Culture, Sports, Science, and Technology (18659435).

Akiro Higashikawa, MD, Taku Saito, MD, PhD, Toshiyuki Ikeda, MD, Satoru Kamekura, MD, PhD, Naohiro Kawamura, MD, PhD, Akinori Kan, MD, Yasushi Oshima, MD, PhD, Shinsuke Ohba, PhD, Naoshi Ogata, MD, PhD, Katsushi Takeshita, MD, PhD, Kozo Nakamura, MD, PhD, Ung-il Chung, MD, PhD, Hiroshi Kawaguchi, MD, PhD: University of Tokyo, Tokyo, Japan.

Address correspondence and reprint requests to Hiroshi Kawaguchi, MD, PhD, Sensory and Motor System Medicine, Faculty of Medicine, University of Tokyo, Hongo 7-3-1, Bunkyo, Tokyo 113-8655, Japan. E-mail: kawaguchi-ort@h.u-tokyo.ac.jp.

Submitted for publication August 9, 2008; accepted in revised form October 13, 2008.

The specificity of type X collagen expression in hypertrophic chondrocytes underlies tight control by transcriptional regulation of gene expression. Runt-related transcription factor 2 (RUNX-2) was originally isolated on the basis of its ability to transactivate the osteoblast-specific osteocalcin gene and is well known as a key molecule for bone formation (13,14). However, recent in vivo studies in mice have revealed that RUNX-2 is the pivotal transcription factor for type X collagen expression and chondrocyte hypertrophy during endochondral ossification (15–20). RUNX-2 is known to function by forming a heterodimer with a cotranscription factor called core-binding factor β (CBFβ) (21).

In a previous study (22,23), we created an experimental OA model by induction of joint instability in mouse knee joints (5). RUNX-2 expression was induced in articular cartilage chondrocytes, followed by type X collagen expression and chondrocyte hypertrophy. Type X collagen expression and cartilage degradation were greatly suppressed in the joints of heterozygous *Runx2*-knockout (Runx2$^{+/-}$) mice as compared with their wild-type littermates. These findings indicate that the RUNX-2–type X collagen signal is likely to play a crucial role in pathologic skeletal disorders, such as OA, as well as in physiologic skeletal growth and repair. Although RUNX-2 has been reported to activate the promoter of the mouse Col10a1 gene directly via its putative RUNX-2 binding motifs (20), the mechanism of transcriptional regulation of the human COL10A1 gene by RUNX-2 remains unknown. Hence, aiming at clinical application of this signal to treatments of skeletal growth retardation, bone fracture, and OA, in this study we investigated the mechanism underlying the transcriptional regulation of human COL10A1 by RUNX-2 in human cells.

MATERIALS AND METHODS

Animals. All experiments were performed according to a protocol approved by the Animal Care and Use Committee of the University of Tokyo. Wild-type and heterozygous *Runx2*-deficient mice with the *lacZ* gene inserted at the site of the *Runx2* gene deletion (Runx2$^{+/\Delta lacZ}$) were maintained on a C57BL/6 background and were fed a standard rodent diet (CE-2; Clea, Tokyo, Japan).

Bone fracture experiment. A transverse osteotomy was created using a bone saw at the midshaft in the left femur of 8-week-old male Runx2$^{+/\Delta lacZ}$ mice, and was internally stabilized with an intramedullary nail using the inner pin of a 22-gauge spinal needle, as previously described (24–26). For histologic analyses, animals were killed by CO_2 asphyxiation 9 days after surgery, and femurs were excised.

Histologic analysis. Excised tibial limbs and femurs were fixed in 4% formaldehyde buffered with phosphate buffered saline (pH 7.4) for 1 hour at 4°C and rinsed 3 times with washing buffer (0.1*M* sodium phosphate, 0.02% Nonidet P40, 0.01% deoxycholic acid, and 2 m*M* $MgCl_2$ [pH 7.4]). To detect β-galactosidase activity, tibial limbs and femurs were subsequently stained with X-Gal staining buffer (1 mg/ml X-Gal, 5 m*M* potassium ferricyanide, and 5 m*M* potassium ferrocyanide buffered with the washing buffer described above) for 36 hours. The femurs were additionally decalcified for 2 weeks with 10% EDTA (pH 7.4) at 4°C. After dehydration with an increasing concentration of ethanol and embedding in paraffin, they were sectioned into 4-μm slices. For immunohistochemistry, after treatment with 25 μg/ml hyaluronidase for 1 hour, sections were incubated overnight with rabbit polyclonal antibodies to rat type X collagen or with nonimmune serum (1:500 dilution; LSL, Tokyo, Japan). Localizations were detected with a horseradish peroxidase–conjugated secondary antibody (Promega, Madison, WI).

Construction of expression vectors. Full-length human RUNX-2 (accession no. NM_004348) complementary DNA (cDNA) and CBFβ (accession no. NM_022845) cDNA were amplified by polymerase chain reaction (PCR) and cloned into pCMV-HA (Clontech, Palo Alto, CA). RUNX-2 (accession no. NM_009820) cDNA and cDNA for a dominant-negative mutant of RUNX-2 (dnRUNX-2) were cloned into pMx vectors (27). A vector expressing dnRUNX-2 was generated by the form which contains the runt domain with N-terminal domain of RUNX-2 and lacks the C-terminal region, as previously described (19). Production of retrovirus vectors was performed as previously described (28,29). Plat-E cells (2×10^6) were plated in 60-mm dishes and transfected with 2 μg of pMx vector using FuGene 6 (Roche, Mannheim, Germany). After 24 hours, the medium was replaced with fresh medium, which was collected and used as the retrovirus supernatant 48 hours after transfection. The blasticidin resistance gene was inserted into the pMx vector of RUNX-2 and that of dnRUNX-2 for selection of stable cells.

Cell cultures. HeLa cells, HuH7 cells, COS-7 cells (RIKEN Cell Bank, Tsukuba, Japan), and OUMS27 cells (Health Science Research Resources Bank, Tokyo, Japan) were cultured in high-glucose Dulbecco's modified Eagle's medium (DMEM) with 10% fetal bovine serum (FBS). ATDC-5 cells (RIKEN Cell Bank) were grown and maintained in DMEM–Ham's F-12 (1:1) with 5% FBS. To induce hypertrophic differentiation, ATDC-5 cells were cultured in the presence of insulin–transferrin–sodium selenite supplement (Sigma, St. Louis, MO) for 3 weeks, and then with α-minimum essential medium/5% FBS with 4 m*M* inorganic phosphate for 2 days, as previously described (30). For generation of the stable cell lines, 3×10^5 ATDC-5 cells were plated and cultured in 60-mm dishes for 1 day, and the retrovirus supernatant was added to the cells with Polybrene (8 μg/ml final concentration). After 2 days, the cells were passaged into 100-mm dishes and cultured with medium containing 10 μg/ml blasticidin until confluency. For alizarin red staining, cultured cells were fixed in 10% buffered formalin and stained for 10 minutes with 2% alizarin red S (pH 4.0) (Sigma). For von Kossa's staining, cells were fixed with 100% ethanol for 15 minutes and stained with 5% silver nitrate solution under ultraviolet light for 5 minutes.

Reverse transcriptase–PCR (RT-PCR) and real-time RT-PCR analyses. Total RNA from cells was isolated with an RNeasy Mini kit, according to the recommendations of the manufacturer (Qiagen, Hilden, Germany), and 1 aliquot (1 μg) was reverse-transcribed with a QuantiTect Reverse Transcription kit (Qiagen) to make single-stranded cDNA. For RT-PCR, cDNA was amplified for 30 cycles in a PCR thermal cycler using Takara Ex *Taq* (Takara Bio, Shiga, Japan) and the following primer pairs: for the N-terminal region of RUNX-2, 5′-GCAAGATGAGCGACGTGAG-3′ and 5′-GTCCGCGATGATCTCCAC-3′; for the C-terminal region of RUNX-2, 5′-CCCAGCCACCTTTACCTACA-3′ and 5′-TATGGAGTGCTGCTGGTCTG-3′; and for β-actin, 5′-AGATGTGGATCAGCAAGCAG-3′and5′-GCGCAAGTTAGGTTTTGTCA-3′.

Real-time RT-PCR was performed with an ABI Prism 7000 Sequence Detection System (Applied Biosystems, Foster City, CA) using QuantiTect SYBR Green PCR Master Mix, according to the recommendations of the manufacturer (Qiagen). All reactions were run in triplicate. After data collection, the messenger RNA (mRNA) copy number of a specific gene in total RNA was calculated using a standard curve generated with serially diluted plasmids containing PCR amplicon sequences and normalized to rodent total RNA (Applied Biosystems) with mouse β-actin as an internal control. Standard plasmids were synthesized with a TOPO TA cloning kit, according to the recommendations of the manufacturer (Invitrogen, Carlsbad, CA). PCR amplification was performed using the following primer pairs: for type X collagen, 5′-CATAAAGGGCCCACTTGCTA-3′ and 5′-TGGCTGATATTCCTGGTGGT-3′; and for β-actin, 5′-AGATGTGGATCAGCAAGCAG-3′ and 5′-GCGCAAGTTAGGTTTTGTCA-3′.

Sequence search of COL10A1 promoters. A sequence search for the RUNX-2 binding motif was performed using Vector NTI (Invitrogen). To search sequences that were conserved between the human and mouse COL10A1 proximal promoters, we performed a BLASTN search (31) against the mouse genomic plus transcript database using a 4.5-kb fragment of the human COL10A1 5′-end flanking region.

Luciferase assay. The human COL10A1 promoter region from −4,459 bp to +39 bp relative to the transcription start site was obtained by PCR using human genomic DNA as a template and was cloned into the pGL3-Basic vector (Promega). Deletion and mutation constructs were created by PCR. Tandem repeat constructs were created by ligating double-stranded oligonucleotides into the pGL3-Basic vector. Transfection of HeLa, HuH7, OUMS27, and ATDC-5 cells was performed in triplicate in 48-well plates using FuGene 6 with plasmid DNA (100 ng of pGL3 reporter vector, 50 ng of effector vector, and 4 ng of pRL-TK vector [Promega]) for internal control per well. Cells were harvested 48 hours after transfection. Luciferase assay was performed with a dual luciferase reporter assay system (Promega) using a GloMax 96 microplate luminometer (Promega). Results were shown as the ratio of firefly activity to *Renilla* activity.

Electrophoretic mobility shift assay (EMSA). Nuclear extracts were obtained from COS-7 cells overexpressing empty vector, RUNX-2, or the combination of RUNX-2 and CBFβ 48 hours after transfection using NE-PER, according to the recommendations of the manufacturer (Pierce, Rockford, IL). Each expression vector was transfected using FuGene 6. EMSA was carried out using a DIG Gel Shift kit, according to the recommendations of the manufacturer (Roche). Binding reactions were incubated for 30 minutes at room temperature. For competition analyses, a 100-fold excess of unlabeled competitor probe was included in the binding reaction. For the supershift experiments, 1 μl of anti–RUNX-2 antibody (M-70 X; Santa Cruz Biotechnology, Santa Cruz, CA) was added after 30 minutes of binding reaction, and the reaction was incubated for an additional 30 minutes at room temperature. Samples were loaded onto Novex 6% Tris–borate–EDTA gels (Invitrogen) and electrophoresed at 100V for 60 minutes.

Chromatin immunoprecipitation (ChIP) assay. A ChIP assay was performed with a OneDay ChIP kit, according to the recommendations of the manufacturer (Diagenode, Liège, Belgium). HuH7 cells were transfected with empty vector and the combination of RUNX-2 and CBFβ using FuGene 6. In vivo crosslinking was performed 48 hours after transfection. To shear genomic DNA, the lysates were then sonicated on ice 10 times for 30 seconds each. For immunoprecipitation, anti–RUNX-2 antibody (M-70 X) and normal rabbit IgG (negative control; Promega) were used.

RESULTS

Localization of RUNX-2 and type X collagen during endochondral ossification. We initially examined the in vivo expression patterns of RUNX-2 and type X collagen during endochondral ossification in skeletal growth and repair using specimens of limb cartilage from neonatal mice and bone fracture callus from adult mice (Figure 1). Due to the lack of appropriate and sensitive antibodies or riboprobes to examine RUNX-2 localization in wild-type mouse cartilage tissue, we used X-Gal staining in heterozygous *Runx2*-deficient mice with the *lacZ* gene insertion at the *Runx2*-deletion site ($Runx2^{+/lacZ}$) (32). RUNX-2 was widely expressed in cartilage and bone areas, but was expressed most strongly in hypertrophic chondrocytes in both specimens. Strong RUNX-2 expression was well colocalized with the area of positive immunostaining with type X collagen, consistent with the results we previously reported for OA cartilage (22) and confirming the molecular interaction between RUNX-2 and type X collagen during endochondral ossification.

Functional role of RUNX-2 in type X collagen expression and terminal differentiation of cultured chondrocytes. To investigate the function of RUNX-2 during endochondral ossification, we examined the effects of gain and loss of function of RUNX-2 on mouse chondrogenic ATDC-5 cells that were cultured in differentiation medium (30). For the gain-of-function analysis, we established stable lines of ATDC-5 cells overexpressing RUNX-2 or the empty vector through retroviral

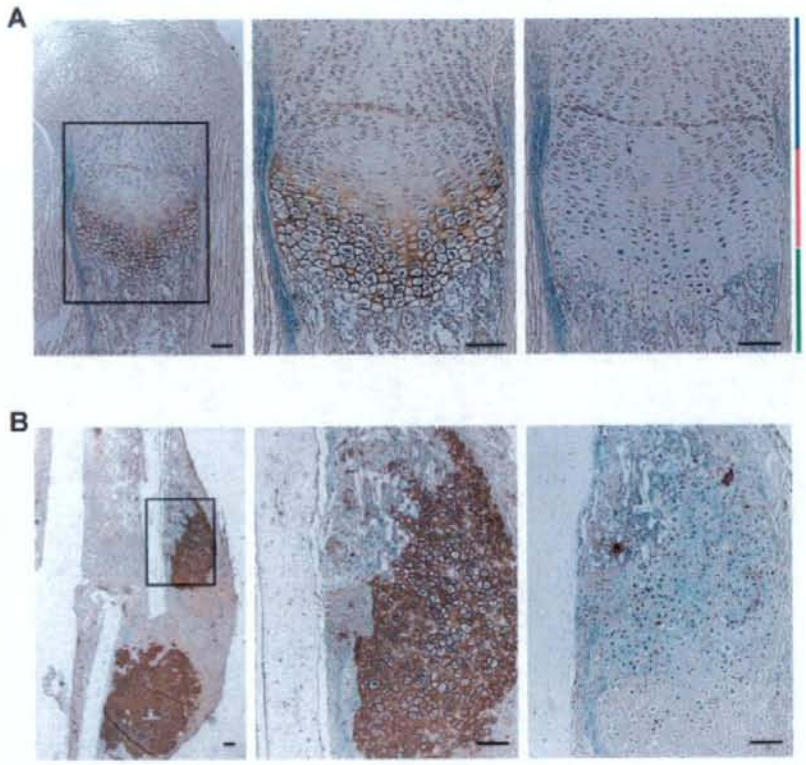

Figure 1. Expression of runt-related transcription factor 2 (RUNX-2) and type X collagen in **A**, the proximal tibial limb cartilage of 1-day-old neonatal mice and **B**, the bone fracture callus of 8-week-old adult mice 9 days after osteotomy at the femur midshaft. Specimens from heterozygous *Runx2*-deficient mice with the RUNX-2 promoter and *lacZ* gene knockin at the *Runx2* deletion site ($Runx2^{+/lacZ}$ mice) were stained with X-Gal and antibody to type X collagen (left and middle) or with X-Gal and nonimmune control serum (right). RUNX-2 localization is shown as blue X-Gal staining to detect β-galactosidase activity. Type X collagen localization is shown as brown immunostaining with an antibody to type X collagen. The middle and right panels show higher-magnification views of the boxed areas in the left panels. The blue, red, and green bars in **A** indicate layers of proliferative zone, hypertrophic zone, and bone area, respectively. Bars = 100 μm.

transfection and found that the type X collagen mRNA level as well as the terminal differentiation determined by alizarin red and von Kossa's stainings were potently stimulated by RUNX-2 overexpression (Figure 2A).

Next, to determine the effects of loss of function of RUNX-2, we established stable lines of ATDC-5 cells overexpressing a dominant-negative mutant of RUNX-2 that lacks the C-terminal region (19), which were cultured in differentiation medium (Figure 2B). The type X collagen mRNA level and the intensity of the stainings were decreased by the overexpression, indicating that RUNX-2 is a crucial factor for type X collagen expression and terminal differentiation of chondrocytes.

Transactivation of the human COL10A1 promoter by RUNX-2 and identification of the responsive element. To examine the mechanism underlying the induction of type X collagen expression by RUNX-2 in humans, we initially compared sequences of the 4.5-kb fragment of the 5′-end flanking region of the human COL10A1 gene with the corresponding mouse genes

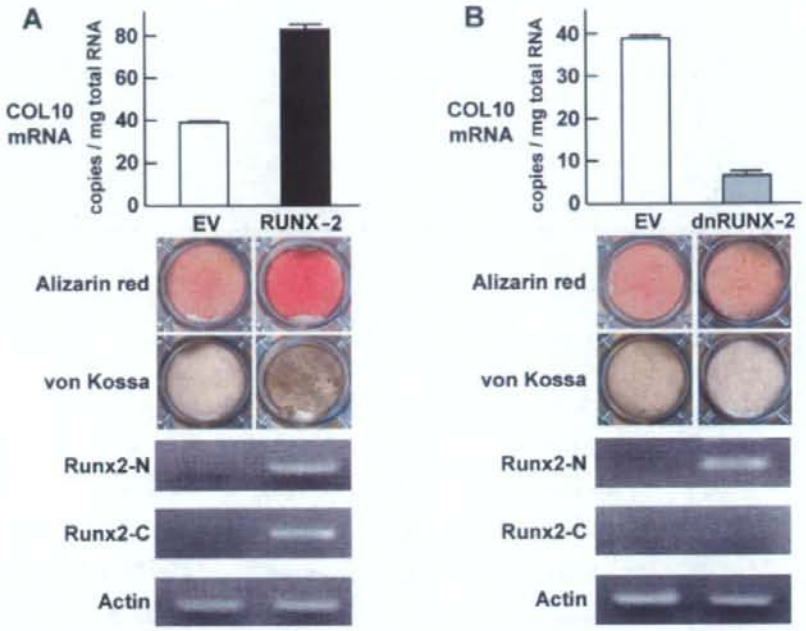

Figure 2. Effect of gain and loss of function of runt-related transcription factor 2 (RUNX-2) on type X collagen (COL10) expression and terminal differentiation in cultured mouse chondrogenic ATDC-5 cells. **A,** Type X collagen mRNA level, determined by real-time reverse transcriptase–polymerase chain reaction (RT-PCR), and alizarin red and von Kossa's staining in stable lines of ATDC-5 cells retrovirally transfected with empty vector (EV; control) or with RUNX-2 after culture for 3 weeks with insulin–transferrin–sodium selenite and for 2 days with inorganic phosphate. **B,** Type X collagen mRNA level, determined by RT-PCR, and alizarin red and von Kossa's staining in stable lines of ATDC-5 cells retrovirally transfected with empty vector or with dominant-negative RUNX-2 (dnRUNX-2), which contains the N-terminal region (Runx2-N), but not the C-terminal region (Runx2-C) of RUNX-2, under the same culture conditions as in **A.** Gene expression of RUNX-2 and dnRUNX-2 was confirmed by RT-PCR analysis using 2 primer sets for the N-terminal region and the C-terminal region of RUNX-2. Bars show the mean and SD of 3 wells per group.

(Figure 3A). The sequences were substantially different, except for 2 regions that were ≥70% conserved between the species.

We then analyzed the promoter activity of the human COL10A1 gene using 3 human cell lines, epithelial HeLa cells, hepatic HuH7 cells, and chondrogenic OUMS27 cells, that were transfected with a luciferase reporter gene construct containing the 4.5-kb fragment of the 5'-end flanking region of the COL10A1 gene and the series of deletion fragments (Figure 3B). The transcription activity determined by the luciferase reporter assay was enhanced by cotransfection with RUNX-2 and more potently by cotransfection with both RUNX-2 and the coactivator CBFβ as compared with the control empty vector, confirming activation of the COL10A1 promoter by RUNX-2 and enhancement by the CBFβ cotransfection in all cell lines. Deletion analysis by a series of 5'-deletion constructs identified the responsive region to RUNX-2 as being between −81 bp and −76 bp, containing a putative RUNX-2 binding sequence (TGAGGG), which is similar to that identified in the promoter region of human interleukin-3 (TGTGGG) (33). This was within the highly conserved region in the comparative mapping described above (Figure 3A).

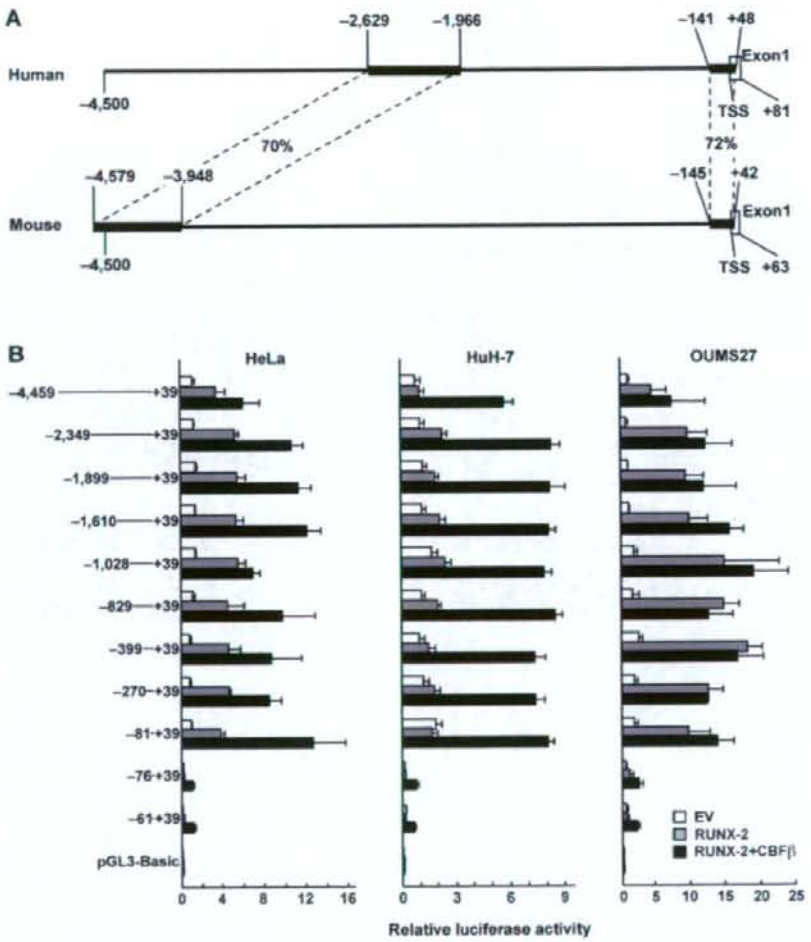

Figure 3. **A,** Comparison of sequences of COL10A1 proximal promoter regions in human and mouse genes. The 4.5-kb fragment of the human 5′-end flanking region was compared with the mouse genomic plus transcript database. **B,** Luciferase assays for human COL10A1 promoter activity induced by transfection with RUNX-2 and identification of the responsive region by deletion analysis in human cells. Three human cell lines, epithelial HeLa cells, hepatic HuH7 cells, and chondrogenic OUMS27 cells, transfected with luciferase reporter constructs containing a 5′-end flanking region of the human COL10A1 gene (from −4,459 bp to +39 bp relative to the transcription start site) and the series of deletion fragments were cotransfected with empty vector (control), RUNX-2 alone, or RUNX-2 and core-binding factor β (CBFβ). Bars show the mean and SD relative luciferase activity (ratio of firefly activity to *Renilla* activity) of 3 wells per group. TSS = transcription start site (see Figure 2 for other definitions).

We therefore prepared the 30-bp element (from −89 to −60 bp) containing the identified region for further analyses, and called it the hypertrophy box (HY box) (Figure 4). To determine the core responsive element in the HY box, we performed site-directed mutagenesis analysis of the luciferase assay by creating 3

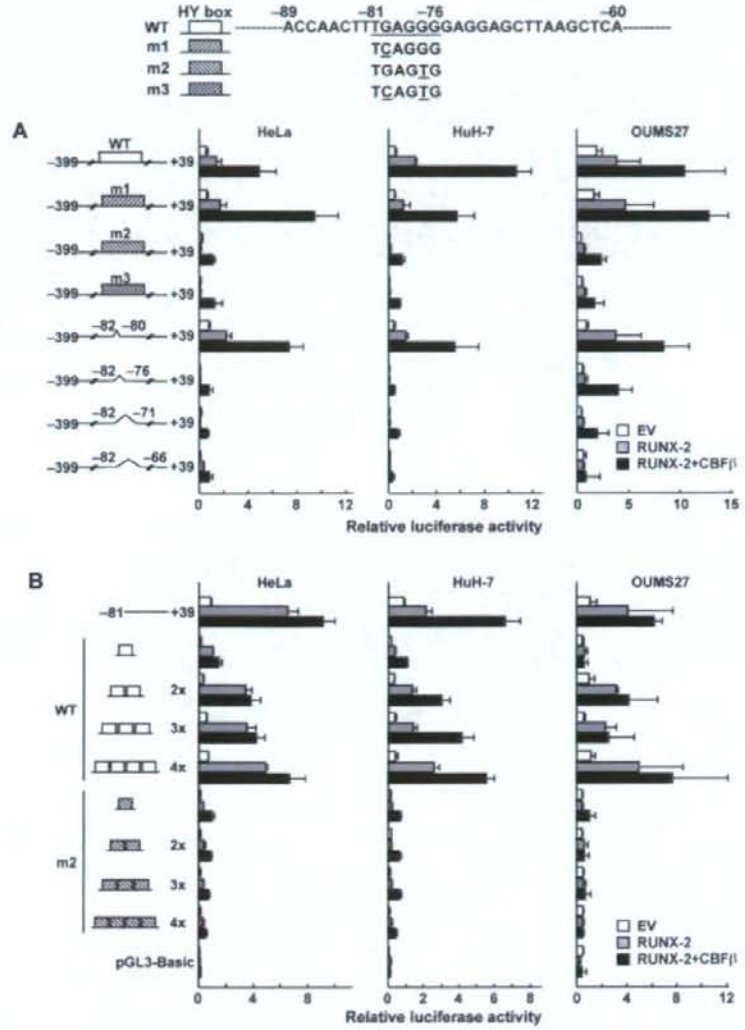

Figure 4. Luciferase assays for determination of the core responsive element in the hypertrophy box (HY box; −89 bp to −60 bp) containing the identified responsive region (from −81 bp to −76 bp, underlined) in the human COL10A1 promoter by site-directed mutagenesis (underlined) and deletion, and dose-response analysis of the tandem repeats using 3 human cell lines cotransfected with empty vector (control), RUNX-2 alone, or RUNX-2 and the coactivator core-binding factor β (CBFβ). **A,** Single-base mutations (m1 and m2), a double-base mutation (m3), and 1–15-bp deletions starting at the −81 bp site were created in the HY box of the 5′-end flanking region between −339 bp and +39 bp, and luciferase activity was compared with that in the wild-type (WT) HY box. **B,** Dose-response analysis of the tandem repeats of the WT and the mutated (m2) HY box was performed. Bars show the mean and SD relative luciferase activity of 3 wells per group. See Figure 2 for other definitions.

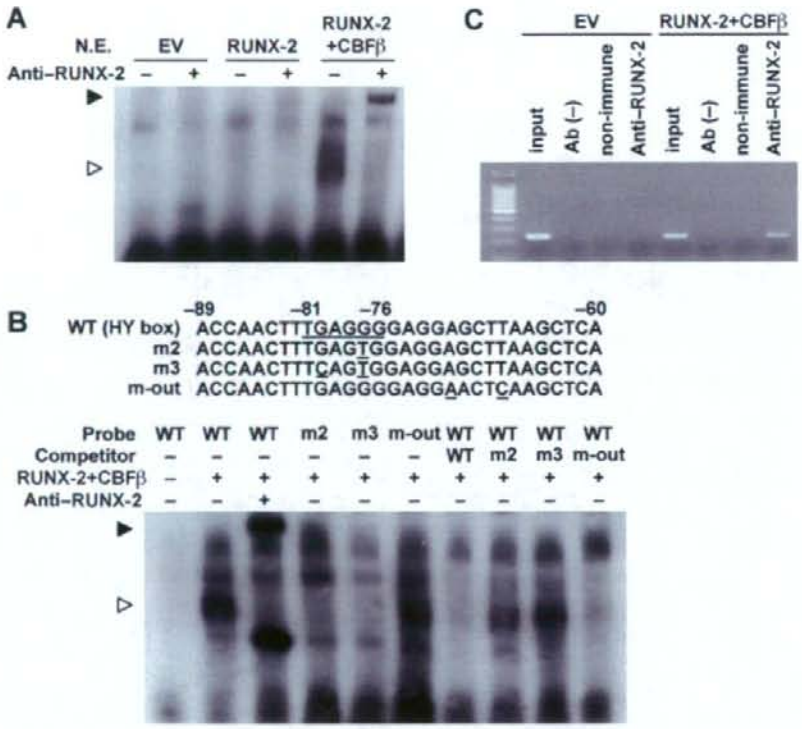

Figure 5. In vitro and in vivo binding of RUNX-2 and the hypertrophy box (HY box). **A,** Electrophoretic mobility shift assay (EMSA) for binding of the digoxigenin-labeled HY box oligonucleotide probe with nuclear extracts (N.E.) of COS-7 cells transfected with empty vector (control), RUNX-2 alone, or RUNX-2 and core-binding factor β (CBFβ). **B,** EMSA for binding of the wild-type (WT) and mutated HY box probes with nuclear extracts of COS-7 cells transfected with RUNX-2 and CBFβ. Mutations (underlined) were created inside (m2 and m3) and outside (m-out) the responsive region (from −81 bp to −76 bp; underlined). Cold competition with a 100-fold excess of unlabeled WT or mutated probes is shown. **C,** Chromatin immunoprecipitation assay for in vivo binding of RUNX-2 and the HY box. Cell lysates of HuH7 cells transfected with empty vector (control) or RUNX-2 and CBFβ were amplified with a primer set (from −113 bp to +119 bp) spanning the HY box before (input) and after immunoprecipitation with an antibody to RUNX-2 or the control nonimmune IgG or in the absence of antibody (Ab [−]). Open arrowheads indicate the shifted bands of the RUNX-2–DNA probe complex; solid arrowheads indicate the bands supershifted by an antibody to RUNX-2. See Figure 2 for other definitions.

mutations in the identified responsive region (mutation 1 at −80 bp, mutation 2 at −77 bp, and mutation 3 at both −80 bp and −77 bp) of the fragment between −339 bp and +39 bp (Figure 4A). Transactivation by RUNX-2 alone and in combination with CBFβ was suppressed by mutation 2 and mutation 3, but not by mutation 1, indicating that the −77 bp site is crucial for the transactivation of COL10A1 by RUNX-2. Luciferase assays by 1–15-bp deletions starting at the −81 bp site in the HY box confirmed that promoter activation by RUNX-2 was suppressed when the −77 bp site was included in the deletions (Figure 4A). Dose-response analysis of tandem repeats of the wild-type and the mutated (mutation 2) HY box clearly revealed that the wild-type HY box responded to RUNX-2 alone and in combination with CBFβ in a repeat number–dependent manner in all cells, while mutation 2 at the −77 bp site markedly suppressed the responses (Figure 4B).

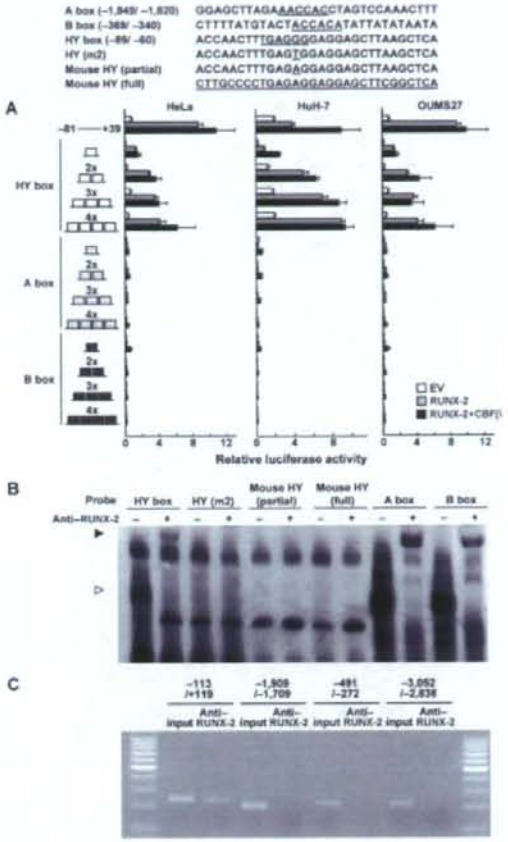

Figure 6. RUNX-2 transactivation of and binding to the A box (from –1849 bp to –1820 bp), B box (from –369 bp to –340 bp), and HY box (from –89 bp to –60 bp) in the human COL10A1 promoter. **A,** Response of luciferase activity to tandem repeats of the HY box, A box, and B box using human cells cotransfected with empty vector (control), RUNX-2 alone, or RUNX-2 and core-binding factor β (CBFβ). Bars show the mean and SD relative luciferase activity of 3 wells per group. **B,** Electrophoretic mobility shift assay (EMSA) for specific binding of digoxigenin-labeled oligonucleotide probes of the HY box, A box, and B box with nuclear extracts of COS-7 cells transfected with RUNX-2 and CBFβ. In addition to the 3 human elements, binding of 3 mutated HY box probes (m2) that mutated to the corresponding mouse sequence only at −77 bp in the core responsive region (mouse HY [partial]), and that fully mutated to the corresponding mouse sequence (mouse HY [full]) were examined. Open arrowheads indicate shifted bands of the RUNX-2–DNA complex; solid arrowheads indicate bands supershifted by an antibody to RUNX-2. **C,** Chromatin immunoprecipitation assay for in vivo binding of RUNX-2 with the human elements. Cell lysates of HuH7 cells transfected with RUNX-2 and CBFβ were amplified with a primer set spanning the HY box (from –113 bp to +119 bp), A box (from –1,909 bp to –1,709 bp), or B box (from –491 bp to –272 bp), or a primer set that did not include a RUNX-2 binding motif (from –3,052 bp to –2,838 bp) before (input) and after immunoprecipitation with an antibody to RUNX-2.

Specific binding of RUNX-2 to the HY box. We further examined in vitro and in vivo binding of RUNX-2 to the HY box by EMSA and ChIP assay, respectively. EMSA showed complex formation by the HY box oligonucleotide probe and nuclear extracts of COS-7 cells transfected with RUNX-2 and CBFβ (Figure 5A). The complex was barely detected with nuclear extracts of cells transfected with RUNX-2 alone, suggesting that CBFβ is necessary for binding. However, supershift of the complex by an antibody to RUNX-2

confirmed the binding of RUNX-2 to the HY box (Figure 5A).

Mutagenesis analyses in the HY box oligonucleotide probe showed that complex formation was abolished by the mutations inside the identified responsive region (from −81 bp to −76 bp) (mutations 2 and 3 in Figure 4), but not by mutations outside the region (Figure 5B). Cold competition with an excess amount of the unlabeled wild-type and outside mutation probes suppressed complex formation, while competition with the unlabeled inside mutation probes did not affect it (Figure 5B). These results demonstrate the specific binding between RUNX-2 and the identified responsive region (from −81 bp to −76 bp) of the HY box.

ChIP assay showed in vivo binding of RUNX-2 to the COL10A1 promoter regulatory region, including the HY box, in the presence of CBFβ (Figure 5C). Specificity was confirmed as RUNX-2 because it was not immunoprecipitated in the absence of the antibody or by the negative control nonimmune IgG.

Involvement of other RUNX-2 binding motifs in the activation of the human COL10A1 promoter by RUNX-2. Next, we screened for other possible RUNX-2 binding motifs with the putative consensus sequences (20) in the 4.5-kb fragment of the 5′-end flanking region of the human COL10A1 promoter. Of the 6 identified regions, we selected the 2 most probable regions. The region from −1,839 bp to −1,834 bp was shown by comparative genomic analysis to correspond to the core responsive element of RUNX-2 in the mouse Col10a1 promoter identified in a previous study (20), and the region from −357 to −352 was the most proximal to the transcription start site of the 6 regions. We then prepared the 30-bp elements that included these 2 regions for further analyses, and called them A box (from −1,849 bp to −1,820 bp) and B box (from −369 bp to −340 bp) (Figure 6).

When we compared the dose-response effects of the tandem repeats on luciferase activity using the 3 human cell lines as described above, neither the A box nor the B box responded to RUNX-2 alone or to RUNX-2 in combination with CBFβ regardless of the number of repeats, in contrast to the HY box, which showed potent repeat number–dependent increases (Figure 6A). In addition to the 3 human elements, we examined binding of the partially or fully mutated HY box probe to the corresponding mouse sequence with RUNX-2 by EMSA. None of the mutated HY box probes formed a complex with the nuclear extract of RUNX-2 and CBFβ-transfected cells (Figure 6B), similar to mutation 2 in Figure 5B. However, both A box and B box oligonucleotide probes did form complexes with the nuclear extracts, which were supershifted by addition of an antibody to RUNX-2, indicating the specific binding of RUNX-2 to all human wild-type elements: HY box, A box, and B box (Figure 6B). More interestingly, when in vivo binding of RUNX-2 to the 3 elements was examined by ChIP assay using human HuH7 cells, RUNX-2 bound to the COL10A1 promoter region that included the HY box, but not to the region including the A box or B box or to the region without the putative RUNX-2 binding motif (Figure 6C).

The results of luciferase assay, EMSA, and ChIP suggested that the HY box was the principal responsive element of RUNX-2 under specific epigenetic environments in human cells. In fact, when we used mouse chondrogenic ATDC-5 cells instead of human cells for the luciferase assays, neither RUNX-2 alone nor a combination of RUNX-2 and CBFβ affected COL10A1 promoter activity. (Data are available online at http://www.h.u-tokyo.ac.jp/ortho/Supplemental_Figures.pdf.) Interestingly, however, there was a decrease in the region between −81 bp and −76 bp in not only RUNX-2–induced activity, but also basal promoter activity. Furthermore, luciferase assays of the tandem repeats of the human elements showed a moderate but repeat number–dependent increase in HY box activity in ATDC-5 cells whether or not they were transfected with RUNX-2, although neither the mutated HY box (mutation 2), A box, nor B box showed the response. (Data are available online at http://www.h.u-tokyo.ac.jp/ortho/Supplemental_Figures.pdf.) Hence, the HY box may also function as a basal responsive element for various transcriptional stimulations regardless of species.

DISCUSSION

The present study showed that human COL10A1 promoter activity was enhanced by RUNX-2 alone and was enhanced even more potently by RUNX-2 in combination with the coactivator CBFβ, and further identified the HY box as the principal and specific responsive element in the 3 human cell lines. Although this is the first study to identify the promoter element responsive to RUNX-2 in the human COL10A1 gene, RUNX-2 binding sites have previously been identified at more distal regions in the mouse Col10a1 promoter (20), which is not within the highly conserved region between mouse and human genes (Figure 3A). The human promoter region that corresponds to the mouse responsive element (A box) showed little response to RUNX-2 and did not show in vivo binding with RUNX-2 in

human cells (Figures 6A and C). The mouse promoter region that corresponds to the human HY box did not bind to RUNX-2 (Figure 6B), and the human HY box did not respond to RUNX-2 in mouse ATDC-5 cells. (Data are available online at http://www.h.u-tokyo.ac.jp/ortho/Supplemental_Figures.pdf.) These findings indicate that there are different mechanisms of type X collagen transactivation by RUNX-2 in humans and mice, and demonstrate that RUNX-2 binds to and activates the HY box in the specific microenvironment in human cells.

Nevertheless, the present study showed the colocalization of RUNX-2 and type X collagen in mouse specimens (Figure 1) and the induction of endogenous type X collagen expression by RUNX-2 in mouse cells (Figure 2). Our study had inevitable limitations, since neither human samples during endochondral ossification nor human chondrogenic cell lines that undergo hypertrophic differentiation are available. Indeed, the endogenous type X collagen induction in mouse cells by RUNX-2 shown in Figure 2 may not be due to transactivation of the mouse HY box, but to transactivation of the responsive element identified in a previous mouse study (20). However, mutations in the RUNX-2 gene cause cleidocranial dysplasia in both humans and mice (32,34,35). In addition, mutations in the COL10A1 gene cause skeletal abnormalities similar to Schmid-type metaphyseal chondrodysplasia in both species (9–12). We therefore believe that RUNX-2 and type X collagen play a role in endochondral ossification in humans as well as in mice.

The temporal and spatial specificity of type X collagen expression has been shown to be under the tight control of positive and negative regulators. In contrast to the positive regulator RUNX-2, parathyroid hormone (PTH) and PTH-related protein (PTHrP) are known to be crucial inhibitors of transcription (36–38). Previous searches in the human COL10A1 promoter have located a regulatory region between −2,410 bp and −1,875 bp upstream of the transcription start site, the activity of which was suppressed by PTH/PTHrP (38–42). In the central part of the region, a functional activator protein 1 (AP-1) site was identified between −2,144 bp and −2,135 bp as a responsive region of FosB and Fra-1 (42). Another enhancer region was identified between −2,273 bp and −2,244 bp, although the related transcription factor remains unknown (41). The deletion analysis of the luciferase assay that was performed in the present study, however, failed to detect a decrease in activity between −2,349 bp and −1,899 bp, which contains the 2 above-mentioned regions, with or without RUNX-2 transfection in any cell line (Figure 3B), indicating a different mechanism of RUNX-2 transcriptional regulation than of PTH/PTHrP and AP-1 transcriptional regulation in humans.

For the examination of RUNX-2 localization in the limb cartilage and the bone fracture callus, we used X-Gal staining in heterozygous *Runx2*-deficient mice with *lacZ* gene insertion at the *Runx2*-deletion site ($Runx2^{+/lacZ}$ mice) (32). This is because neither antibodies nor riboprobes worked appropriately in the localization of RUNX-2 by immunostaining or in situ hybridization, respectively, of the tissue of wild-type mice. Our preliminary studies confirmed that the $Runx2^{+/lacZ}$ mice showed normal skeletal phenotypes, except that they exhibited a dysplastic clavicle, which is typical of cleidocranial dysplasia, as previously reported (32) (Details are available online at http://www.h.u-tokyo.ac.jp/ortho/Supplemental_Figures.pdf.) Their growth plate phenotypes were also comparable with those of their wild-type littermates before and after birth. In addition, fracture callus formation and type X collagen expression in the callus were similar between the 2 genotypes.

These findings indicate that the RUNX-2 haploinsufficiency in $Runx2^{+/lacZ}$ mice did not cause abnormalities in skeletal growth or repair, confirming the adequacy of using $Runx2^{+/lacZ}$ mice instead of wild-type mice for the analysis. However, in a previous study in which we created an experimental OA model by induction of knee joint instability, $Runx2^{+/lacZ}$ mice exhibited suppression of type X collagen expression and degradation in joint cartilage (22). The fact that RUNX-2 haploinsufficiency prevented OA progression without affecting physiologic skeletal growth and repair suggests that RUNX-2–related signaling can be a therapeutic target of this disorder without severe skeletal side effects.

The HY box is indeed a core promoter element in the human COL10A1 gene responsive to RUNX-2 in human cells. However, basal luciferase activity without RUNX-2 transfection was also decreased in the region between −81 bp and −76 bp in the HY box not only in mouse ATDC-5 cells, but also in 3 human cell lines (Figure 3B), although not to as great an extent as RUNX-2–induced activity. Furthermore, the site-directed mutagenesis (Figure 4A) and tandem repeat experiments (Figure 4B) in the HY box showed a decrease and a repeat number–dependent increase, respectively, of basal luciferase activity in human cells without RUNX-2 transfection. These indicate that the HY box may also function as a potent universal enhancer in the human COL10A1 promoter, responding to

various transcriptional stimulations besides RUNX-2 in human cells. Considering that chondrocyte hypertrophy is a crucial step for skeletal growth, repair, and OA progression, the HY box will be useful in the comprehensive screening of transcription factors or cofactors for COL10A1 transactivation and chondrocyte hypertrophy, which might be therapeutic targets for skeletal growth retardation, fractures, and OA.

ACKNOWLEDGMENTS

We thank Dr. Michael Owen (GlaxoSmithKline, London, UK) for providing Runx2$^{-/lacZ}$ mice. We also thank Reiko Yamaguchi and Hajime Kawahara for excellent technical assistance.

AUTHOR CONTRIBUTIONS

Dr. Kawaguchi had full access to all of the data in the study and takes responsibility for the integrity of the data and the accuracy of the data analysis.

Study design. Higashikawa, Saito, Ohba, Takeshita, Nakamura, Chung, Kawaguchi.

Acquisition of data. Higashikawa, Saito, Kamekura, Kan, Oshima.

Analysis and interpretation of data. Higashikawa, Ikeda, Ogata, Takeshita, Chung, Kawaguchi.

Manuscript preparation. Higashikawa, Takeshita, Kawaguchi.

Statistical analysis. Higashikawa, Saito, Kawamura, Kawaguchi.

REFERENCES

1. Kronenberg HM. Developmental regulation of the growth plate. Nature 2003;423:332–6.
2. Shapiro F. Bone development and its relation to fracture repair: the role of mesenchymal osteoblasts and surface osteoblasts. Eur Cell Mater 2008;15:53–76.
3. Von der Mark K, Kirsch T, Nerlich A, Kuss A, Weseloh G, Gluckert K, et al. Type X collagen synthesis in human osteoarthritic cartilage: indication of chondrocyte hypertrophy. Arthritis Rheum 1992;35:806–11.
4. Boos N, Nerlich AG, Wiest I, von der Mark K, Ganz R, Aebi M. Immunohistochemical analysis of type X-collagen expression in osteoarthritis of the hip joint. J Orthop Res 1999;17:495–502.
5. Kamekura S, Hoshi K, Shimoaka T, Chung U, Chikuda H, Yamada T, et al. Osteoarthritis development in novel experimental mouse models induced by knee joint instability. Osteoarthritis Cartilage 2005;13:632–41.
6. Linsenmayer TF, Long F, Nurminskaya M, Chen Q, Schmid TM. Type X collagen and other up-regulated components of the avian hypertrophic cartilage program. Prog Nucleic Acid Res Mol Biol 1998;60:79–109.
7. Rosati R, Horan GS, Pinero GJ, Garofalo S, Keene DR, Horton WA, et al. Normal long bone growth and development in type X collagen-null mice. Nat Genet 1994;8:129–35.
8. Kwan KM, Pang MK, Zhou S, Cowan SK, Kong RY, Pfordte T, et al. Abnormal compartmentalization of cartilage matrix components in mice lacking collagen X: implications for function. J Cell Biol 1997;136:459–71.
9. Jacenko O, Chan D, Franklin A, Ito S, Underhill CB, Bateman JF, et al. A dominant interference collagen X mutation disrupts hypertrophic chondrocyte pericellular matrix and glycosaminoglycan and proteoglycan distribution in transgenic mice. Am J Pathol 2001;159:2257–69.
10. Warman ML, Abbott M, Apte SS, Hefferon T, McIntosh I, Cohn DH, et al. A type X collagen mutation causes Schmid metaphyseal chondrodysplasia. Nat Genet 1993;5:79–82.
11. Wallis GA, Rash B, Sykes B, Bonaventure J, Maroteaux P, Zabel B, et al. Mutations within the gene encoding the α1 (X) chain of type X collagen (COL10A1) cause metaphyseal chondrodysplasia type Schmid but not several other forms of metaphyseal chondrodysplasia. J Med Genet 1996;33:450–7.
12. Chan D, Jacenko O. Phenotypic and biochemical consequences of collagen X mutations in mice and humans. Matrix Biol 1998;17:169–84.
13. Ducy P, Zhang R, Geoffroy V, Ridall AL, Karsenty G. Osf2/Cbfa1: a transcriptional activator of osteoblast differentiation. Cell 1997;89:747–54.
14. Komori T. Regulation of osteoblast differentiation by transcription factors. J Cell Biochem 2006;99:1233–9.
15. Kim IS, Otto F, Zabel B, Mundlos S. Regulation of chondrocyte differentiation by Cbfa1. Mech Dev 1999;80:159–70.
16. Inada M, Yasui T, Nomura S, Miyake S, Deguchi K, Himeno M, et al. Maturational disturbance of chondrocytes in Cbfa1-deficient mice. Dev Dyn 1999;214:279–90.
17. Enomoto H, Enomoto-Iwamoto M, Iwamoto M, Nomura S, Himeno M, Kitamura Y, et al. Cbfa1 is a positive regulatory factor in chondrocyte maturation. J Biol Chem 2000;275:8695–702.
18. Takeda S, Bonnamy JP, Owen MJ, Ducy P, Karsenty G. Continuous expression of Cbfa1 in nonhypertrophic chondrocytes uncovers its ability to induce hypertrophic chondrocyte differentiation and partially rescues Cbfa1-deficient mice. Genes Dev 2001;15:467–81.
19. Ueta C, Iwamoto M, Kanatani N, Yoshida C, Liu Y, Enomoto-Iwamoto M, et al. Skeletal malformations caused by overexpression of Cbfa1 or its dominant negative form in chondrocytes. J Cell Biol 2001;153:87–100.
20. Zheng Q, Zhou G, Morello R, Chen Y, Garcia-Rojas X, Lee B. Type X collagen gene regulation by Runx2 contributes directly to its hypertrophic chondrocyte-specific expression in vivo. J Cell Biol 2003;162:833–42.
21. Komori T. Requisite roles of Runx2 and Cbfb in skeletal development. J Bone Miner Metab 2003;21:193–7.
22. Kamekura S, Kawasaki Y, Hoshi K, Shimoaka T, Chikuda H, Maruyama Z, et al. Contribution of runt-related transcription factor 2 to the pathogenesis of osteoarthritis in mice after induction of knee joint instability. Arthritis Rheum 2006;54:2462–70.
23. Kawaguchi H. Endochondral ossification signals in cartilage degradation during osteoarthritis progression in experimental mouse models. Mol Cells 2008;25:1–6.
24. Kugimiya F, Kawaguchi H, Kamekura S, Chikuda H, Ohba S, Yano F, et al. Involvement of endogenous bone morphogenetic protein (BMP) 2 and BMP6 in bone formation. Calcif Tissue Int 2005;280:35704–12.
25. Yamada T, Kawano H, Koshizuka Y, Fukuda T, Yoshimura K, Kamekura S, et al. Carminerin contributes to chondrocyte calcification during endochondral ossification. Nat Med 2006;12:665–70.
26. Yamakawa K, Kamekura S, Kawamura N, Saegusa M, Kamei D, Murakami M, et al. Association of microsomal prostaglandin E synthase 1 deficiency with impaired fracture healing, but not with bone loss or osteoarthritis, in mouse models of skeletal disorders. Arthritis Rheum 2008;58:172–83.
27. Kitamura T. New experimental approaches in retrovirus-mediated expression screening. Int J Hematol 1998;67:351–9.
28. Morita S, Kojima T, Kitamura T. Plat-E: an efficient and stable system for transient packaging of retroviruses. Gene Ther 2000;7:1063–6.
29. Saito T, Ikeda T, Nakamura K, Chung UI, Kawaguchi H. S100A1

and S100B, transcriptional targets of SOX trio, inhibit terminal differentiation of chondrocytes. EMBO Rep 2007;8:504–9.
30. Magne D, Bluteau G, Faucheux C, Palmer G, Vignes-Colombeix C, Pilet P, et al. Phosphate is a specific signal for ATDC5 chondrocyte maturation and apoptosis-associated mineralization: possible implication of apoptosis in the regulation of endochondral ossification. J Bone Miner Res 2003;18:1430–42.
31. Altschul SF, Gish W, Miller W, Myers EW, Lipman DJ. Basic local alignment search tool. J Mol Biol 1990;215:403–10.
32. Otto F, Thornell AP, Crompton T, Denzel A, Gilmour KC, Rosewell IR, et al. Cbfa1, a candidate gene for cleidocranial dysplasia syndrome, is essential for osteoblast differentiation and bone development. Cell 1997;89:765–71.
33. Uchida H, Zhang J, Nimer SD. AML1A and AML1B can transactivate the human IL-3 promoter. J Immunol 1997;158:2251–8.
34. Mundlos S, Otto F, Mundlos C, Mulliken JB, Aylsworth AS, Albright S, et al. Mutations involving the transcription factor CBFA1 cause cleidocranial dysplasia. Cell 1997;89:773–9.
35. Otto F, Kanegane H, Mundlos S. Mutations in the RUNX2 gene in patients with cleidocranial dysplasia. Hum Mutat 2002;19:209–16.
36. Iwamoto M, Shimazu A, Pacifici M. Regulation of chondrocyte maturation by fibroblast growth factor-2 and parathyroid hormone. J Orthop Res 1995;13:838–45.
37. O'Keefe RJ, Loveys LS, Hicks DG, Reynolds PR, Crabb ID, Puzas JE, et al. Differential regulation of type-II and type-X collagen synthesis by parathyroid hormone-related protein in chick growth-plate chondrocytes. J Orthop Res 1997;15:162–74.
38. Riemer S, Gebhard S, Beier F, Poschl E, von der Mark K. Role of c-fos in the regulation of type X collagen gene expression by PTH and PTHrP: localization of a PTH/PTHrP-responsive region in the human COL10A1 enhancer. J Cell Biochem 2002;86:688–99.
39. Thomas JT, Sweetman WA, Cresswell CJ, Wallis GA, Grant ME, Boot-Handford RP. Sequence comparison of three mammalian type-X collagen promoters and preliminary functional analysis of the human promoter. Gene 1995;160:291–6.
40. Beier F, Vornehm S, Poschl E, von der Mark K, Lammi MJ. Localization of silencer and enhancer elements in the human type X collagen gene. J Cell Biochem 1997;66:210–8.
41. Chambers D, Young DA, Howard C, Thomas JT, Boam DS, Grant ME, et al. An enhancer complex confers both high-level and cell-specific expression of the human type X collagen gene. FEBS Lett 2002;531:505–8.
42. Gebhard S, Poschl E, Riemer S, Bauer E, Hattori T, Eberspaecher H, et al. A highly conserved enhancer in mammalian type X collagen genes drives high levels of tissue-specific expression in hypertrophic cartilage in vitro and in vivo. Matrix Biol 2004;23:309–22.

DOI 10.1002/art.24376

Errata

In the articles by Valdes et al in the January 2007 and February 2006 issues of *Arthritis & Rheumatism* (pages 137–146 and 533–539, respectively), some information on sample collection and a funding source was omitted. Collection of some of the samples used for genetic association was carried out by Andrew Carr, MD (Nuffield Orthopaedic Centre, Botnar Research Centre, Oxford University, Oxford, UK), and funding was provided by the Norman Collisson Foundation, the Botnar Foundation, and the Lord Nuffield Orthopaedic Trust).

We regret the errors.

SPINE Volume 34, Number 3, pp E110–E114

Radiographic Analysis of the Cervical Spine in Patients With Retro-Odontoid Pseudotumors

Hirotaka Chikuda, MD,* Atsushi Seichi, MD,† Katsushi Takeshita, MD,* Naoki Shoda, MD,* Takashi Ono, MD,* Ko Matsudaira, MD,* Hiroshi Kawaguchi, MD,* and Kozo Nakamura, MD*

Study Design. A retrospective review of 10 consecutive patients with a noninflammatory retro-odontoid pseudotumor.

Objective. To examine the radiographic characteristics in patients with a retro-odontoid pseudotumor and to evaluate the efficacy of posterior fusion.

Summary of Background Data. A retro-odontoid pseudotumor, a reactive fibrocartilaginous mass, is known to develop after chronic atlantoaxial instability; however, one-third of the reported cases showed no overt atlantoaxial instability. The pathomechanism for such "atypical" cases remains unclear, although altered cervical motion secondary to ossification of the anterior longitudinal ligament (OALL) or severe spondylosis has been implicated.

Methods. We reviewed the charts and radiographs of 10 patients with a retro-odontoid pseudotumor who underwent surgery. Preoperative radiographs were evaluated for atlas-dens interval (ADI), presence of OALL, range of motion, and segmental motion adjacent to the atlantoaxial joint. Computed tomography was evaluated for degenerative changes of zygapophysial joints.

Results. There were 6 men and 4 women. Atlantoaxial instability (ADI >4 mm) was observed in 2 patients. ADI was less than 3 mm in 5 patients. Frequent association of OALL (6 patients) and marked decrease in C2 to C7 range of motion (mean, 17.6°; range, 3°–36°) were noted. Ankylosis of O-C1 was observed in 4 patients and C2 to C3 in 6. Severe degenerative change of C2 to C3 zygapophysial joint was observed in 4 patients. The patients underwent occipito-cervical fusion (9 patients) or direct removal of the pseudotumor (1 patient). Postoperative magnetic resonance imaging invariably demonstrated the mass regression.

Conclusion. Retro-odontoid pseudotumors were not always associated with radiographic atlantoaxial instability. Our data indicate that extensive OALL and ankylosis of the adjacent segments are risk factors for the formation of the pseudotumor. Retro-odontoid pseudotumors may develop as an "adjacent segment disease" after altered biomechanics of the cervical spine, especially those in the adjacent segments. Posterior fusion was effective even in cases without radiographic atlantoaxial instability.

Key words: retro-odontoid pseudotumor, atlantoaxial joint, adjacent segment, ossification of the anterior ligament, hyperostosis, myelopathy, range of motion, spinal fusion. **Spine 2009;34:E110–E114**

A noninflammatory retro-odontoid pseudotumor is a reactive fibrocartilaginous mass formed posterior to the odontoid process.[1–3] The retro-odontoid pseudotumor, a rare but increasingly recognized clinical entity, reportedly develops subsequent to chronic atlantoaxial instability. This view has been further supported by the regression of the mass after posterior fusion, which has become the mainstay of the treatment.[4–9] Although retro-odontoid pseudotumors have been frequently associated with atlantoaxial subluxation, we found that about one-third of the cases reported in the literature showed no overt atlantoaxial instability.[2,5,6,9–14] The pathomechanism for such atypical cases remains unclear, although modified stress distribution of the cervical spine, secondary to severe spondylosis or OALL, has been implicated.[15,16] Moreover, it has not been clarified whether posterior fusion aiming at spontaneous mass regression is similarly effective for the patients without radiographic atlantoaxial instability.

To further elucidate the underlying pathomechanism of the disease, we examined the radiographic characteristics of the cervical spine in patients with the retro-odontoid pseudotumors. Special attention was paid to the presence of OALL and the segmental motion adjacent to the atlantoaxial joint (O-C1, C2–C3). We also evaluated the efficacy of posterior fusion surgery.

■ Materials and Methods

After approval of institutional review board, we reviewed the clinical records of 140 patients who underwent surgery for upper cervical lesion at our department between 2000 and 2006. We identified 10 patients with retro-odontoid pseudotumors, and the radiographs of the 10 patients were examined. The diagnosis was made based primarily on magnetic resonance imaging (MRI) that revealed a mass lesion posterior to the odontoid process with substantial cord compression as evidenced by effacement of the subarachnoid space and indentation of the spinal cord. Masses were typically visualized as ranging from isointense to hypointense relative to spinal cord tissue on T1-weighted images and as hypointense regions on T2-weighted images. The diagnosis

From the *Department of Orthopaedic Surgery, Faculty of Medicine, the University of Tokyo, Tokyo, Japan; and †Department of Orthopaedic Surgery, Jichi Medical University, Jichi, Japan.
Acknowledgment date: March 27, 2008. Revision date: July 08, 2008. Acceptance date: July 21, 2008.
The manuscript submitted does not contain information about medical device(s)/drug(s).
No funds were received in support of this work. No benefits in any form have been or will be received from a commercial party related directly or indirectly to the subject of this manuscript.
This study was approved by the Tokyo University Medical Research Ethics Committee.
Address correspondence and reprint requests to Hirotaka Chikuda, MD, Department of Orthopaedic Surgery, Faculty of Medicine, the University of Tokyo, 7–3–1 Hongo, Bunkyo-ku, Tokyo 113-8655, Japan; E-mail: chikuda-tky@umin.ac.jp

Table 1. Scores of the Motor Functions of the Upper and Lower Extremities for Cervical Myelopathy Set by the Japanese Orthopaedic Association (JOA)

Motor function of the upper extremities (upper m-JOA)	
0	Cannot eat with a spoon
1	Can eat with a spoon, but not with chopsticks
2	Can eat with chopsticks, but to a limited degree
3	Can eat with chopsticks, but awkward
4	No disability
Motor function of the lower extremities (lower m-JOA)	
0	Cannot walk
1	Needs cane or aid on flat ground
2	Needs cane or aid only on stairs
3	Can walk without cane or aid, but slowly
4	No disability

was further confirmed by the radiology report. Specimen of the mass was available in 2 patients (patient 1 and 2). Subsequent histologic examination revealed fibrocartilage and degenerative ligamentous tissue. There was no recurrence of the mass lesion during the follow-up period. Inflammatory granulation of the synovium associated with rheumatoid arthritis and retro-odontoid reactive lesions associated with pseudarthrosis of the dens fracture were excluded from this study. All patients had symptoms of progressive myelopathy: hyperreflexia, positive pathologic reflexes, motor weakness in the upper and lower extremities, clumsiness in hands, and gait disturbance. Neurologic status of the patients was evaluated before surgery and at the last follow-up by a senior author (A.S.). Motor function was rated using the motor function scores of the upper and lower extremities for cervical myelopathy set by the Japanese Orthopedic Association (upper and lower m-JOA score) (Table 1). A full score "4" indicates normal function.

All radiographs were viewed using our institution's digital radiography software (Centricity Web-J software ver.1.6.11; GE Yokogawa Medical Systems, Tokyo, Japan). The measurement of the radiographs was performed independently by 2 spine surgeons (H.C. and N.S.) with the program's digital measuring tool. The results of the 2 reviewers were averaged. The atlas-dens interval (ADI) was measured on preoperative flexion-extension radiographs. The atlantoaxial instability was defined as ADI >4 mm, according to the criteria described by White and Panjabi.[17] Lateral radiographs and sagittal computed tomography (CT) reconstructions were evaluated for the presence of OALL. OALL was defined as bony mass anterior to the vertebrae bridging over 2 or more intervertebral disc spaces. Range of motion (ROM) was measured on preoperative flexion-extension radiographs. The representative lines used for the measurement were as follows: the McGregor line, the line passing through the centers of anterior and posterior arches of the atlas, and the line parallel to the endplate of vertebrae. The mobility of each segment was determined by measuring the difference between 2 corresponding points on the tips of the spinous processes on flexion *versus* extension. Ankylosis was defined as absence of motion on both flexion and extension radiographs. CT reconstructions were further evaluated for degenerative change or fusion of the zygapophysial joints. To assess the regression of the pseudotumor, follow-up MRI obtained 1 year after surgery was reviewed. Maximal thickness of the retro-odontoid soft tissue was measured on preoperative and postoperative MRI in T2-weighted sagittal view. Interobserver reliability of radiographic measurement was assessed with inter class coefficient. All statistics were calculated using SPSS, version 13.0 (SPSS Inc., Chicago, IL).

■ Results

There were 6 men and 4 women with a mean age at surgery of 71 years (range, 58–82 years). Mean follow-up was 30 months (range, 12–84 months). Maximal thickness of the retro-odontoid soft tissue was 9.4 ± 1.3 mm (mean ± SD; range, 7.6-11.4 mm). On examination of the radiographic characteristics (Table 2), ADI averaged 3.4 ± 1.9 mm (mean ± SD) in flexion and 1.8 ± 0.9 mm in extension. Only 2 patients showed overt atlantoaxial instability (ADI >4 mm). ADI was less than 3 mm in 5 patients (Figure 1). We found extensive OALL in 6 patients: C2 to C7 in 4 patients, and C3 to C7 and C3 to C5 in 1 patient each. When ROM of the cervical spine was examined, marked decrease in subaxial (C2–C7)

Table 2. Radiographic Characteristics of the Cervical Spine

		ADI (mm)			ROM (°)		Segmental Motion (°)	
Patient No.	Age (Yr), Sex	Flexion	Extension	OALL	O-C2	C2–C7	O-C1	C2–C3
1	58, M	7.0 ± 0.1	3.2 ± 0.3	C2–C7	30 ± 3.0	6 ± 1.5	7 ± 1.0	10 ± 3.0
2	67, F	6.6 ± 0.6	6.2 ± 0	C3–C5	14 ± 9.1	28 ± 3.9	None*	None
3	72, F	3.5 ± 0.7	1.0 ± 0.1	C2–C7	32 ± 0.9	7 ± 0.6	6 ± 1.1	8 ± 3.6
4	71, M	3.4 ± 0.1	1.5 ± 0	—	17 ± 0.4	23 ± 0.7	None	3 ± 0.2
5	82, M	3.3 ± 0.4	2.1 ± 0.3	C2–C7	18 ± 5.3	5 ± 4.9	8 ± 0.1	None
6	81, M	2.8 ± 0.6	1.5 ± 1.0	C2–C7	35 ± 1.7	22 ± 2.6	5 ± 0.8	None†
7	73, F	2.7 ± 0.1	1.9 ± 0.4	—	24 ± 1.1	35 ± 0.2	None	5 ± 2.5†
8	73, M	2.0 ± 0.6	1.7 ± 0.3	C3–C7	8 ± 0.3	11 ± 2.4	None	None†
9	71, F	2.0 ± 0.3	1.7 ± 0.9	—	28 ± 6.2	36 ± 2.8	4 ± 1.6	None
10	64, M	1.0 ± 0.1	0 ± 0	—	24 ± 2.7	3 ± 3.5	15 ± 3.1	None†

Data are shown as mean ± SD. ICC values for radiographic measurement were as follows: ADI in flexion, 0.97; ADI in extension, 0.98; O-C2 ROM, 0.88; C2–C7 ROM, 0.98; O-C1 ROM, 0.96; and C2–C3 ROM, 0.87. The 2 reviewers were in accord regarding the categorical items including presence of OALL and segmental ankylosis.
*Atlanto-occipital assimilation.
†Severe spondylosis of the C2–C3 zygapophyseal joint.